Optics Letters

Single-tube on-beam quartz-enhanced photoacoustic spectroscopy

Huadan Zheng,[1,2] Lei Dong,[1,2,*] Angelo Sampaolo,[3,4] Hongpeng Wu,[1,2,4] Pietro Patimisco,[3] Xukun Yin,[1,2] Weiguang Ma,[1,2] Lei Zhang,[1,2] Wangbao Yin,[1,2] Vincenzo Spagnolo,[3] Suotang Jia,[1,2] and Frank K. Tittel[4]

[1]State Key Laboratory of Quantum Optics and Quantum Optics Devices, Institute of Laser Spectroscopy, Shanxi University, Taiyuan 030006, China
[2]Collaborative Innovation Center of Extreme Optics, Shanxi University, Taiyuan 030006, China
[3]Dipartimento Interateneo di Fisica, Università degli Studi di Bari and Politecnico di Bari, CNR-IFN BARI, Via Amendola 173, Bari 70126, Italy
[4]Department of Electrical and Computer Engineering, Rice University, Houston, Texas 77005, USA
*Corresponding author: donglei@sxu.edu.cn

Received 10 December 2015; revised 19 January 2016; accepted 30 January 2016; posted 1 February 2016 (Doc. ID 255432); published 25 February 2016

Quartz-enhanced photoacoustic spectroscopy (QEPAS) with a single-tube acoustic microresonator (AmR) inserted between the prongs of a custom quartz tuning fork (QTF) was developed, investigated, and optimized experimentally. Due to the high acoustic coupling efficiency between the AmR and the QTF, the single-tube on-beam QEPAS spectrophone configuration improves the detection sensitivity by 2 orders of magnitude compared to a bare QTF. This approach significantly reduces the spectrophone size with respect to the traditional on-beam spectrophone configuration, thereby facilitating the laser beam alignment. A 1σ normalized noise equivalent absorption coefficient of 1.21×10^{-8} cm^{-1} · W/$\sqrt{\text{Hz}}$ was obtained for dry CO_2 detection at normal atmospheric pressure.

OCIS codes: (280.3420) Laser sensors; (300.6430) Spectroscopy, photothermal; (300.6260) Spectroscopy, diode lasers.

http://dx.doi.org/10.1364/OL.41.000978

Photoacoustic spectroscopy (PAS) is one of the most robust and selective techniques for trace gas detection, capable of extremely high detection sensitivities with a compact absorption detection module (ADM) [1]. Quartz-enhanced photoacoustic spectroscopy (QEPAS) is an alternative approach to photoacoustic detection, using a quartz tuning fork (QTF) instead of a microphone as a sharply resonant acoustic transducer [2–4]. It has been widely used in atmospheric monitoring, industrial process control, and agricultural biogas detection by means of light sources spamming from violet light-emitting diodes (LEDs) to the mid-infrared quantum cascade lasers (QCLs) [5–11]. To date, almost all the QEPAS sensors reported in the literature exploit "standard" QTFs, such as those used in clocks and watches. These QTFs have a resonance frequency of ~32.76 kHz and are characterized by a small sensitive area between their prongs (300 μm spacing). This prevents the use of light sources having a beam shape of poor quality, such as stripe diode or fiber-amplified lasers, and radiation sources in the THz spectral region (wavelength >30 μm), due to the difficulty in adequate focalization of the excitation beam between the QTF prongs. The incident radiation must not hit the QTF, as otherwise an undesirable nonzero background arises, which can be several times larger than the thermal noise level of the QEPAS sensor, thereby strongly limiting the final detection sensitivity [12,13]. QTFs with larger prong spacing are therefore mandatory to extend QEPAS operation in the THz range or with poor beam quality lasers. Recently, custom QTFs with prong spacing in the range of 600–800 μm were specially designed and used to address these issues, allowing efficient light beam focusing of THz quantum cascade [14,15] and erbium-doped fiber-amplified lasers [16] through the two prongs of custom QTFs.

Acoustic microresonators (AmRs) are important components that are mounted together with a QTF to improve the performance of QEPAS sensors [4]. An AmR-based QTF is usually referred as a QEPAS spectrophone. To date, two different QEPAS spectrophone configurations, off-beam and on-beam configurations, have been developed [4,17,18]. The on-beam spectrophone configuration has the stronger acoustic coupling efficiency between the QTF and the AmR, offering an optimum signal-to-noise (SNR) gain factor of ~30 [17]. In the on-beam spectrophone configuration, an AmR made of stainless steel tube is cut into two pieces and a QTF is inserted between them. The two half-tubes, positioned on the two sides of the QTF, confine the acoustic waves and drive the QTF prongs to vibrate. However, the insertion of the QTF distorts the resonance mode of acoustic standing waves in the AmR, resulting in an optimal AmR length of $\lambda/2 < L < \lambda$, where λ is the acoustic wavelength [17,19]. Recently the on-beam configuration was implemented with a custom QTF to enhance the detection sensitivity [16]. The full length of the AmR reached 46 mm, and a SNR gain factor of 40 was achieved as compared with a bare custom QTF. Such a long AmR results in challenging laser beam alignment and spectrophone assembly.

0146-9592/16/050978-04$15/0$15.00

In this Letter, we report what we believe is a novel QEPAS technique called single-tube on-beam quartz enhanced photoacoustic spectroscopy (SO-QEPAS) employing a single-tube AmR between the prongs of the custom tuning fork, as shown in Fig. 1(a). The SO-QEPAS spectrophone configuration can be realized due to the large prong spacing of the custom QTF, allowing space of the AmR between the prongs, thus avoiding the cutting of the AmR into two pieces. In this case, the behavior of the single-tube on-beam AmR is similar to that of an ideal 1D acoustic resonator, resulting in a shorter AmR length and further enhancement of the QEPAS signal. The symbols of the geometrical parameters of the SO-QEPAS spectrophone are shown in Figs. 1(b)–1(d), where g and T represent the prong spacing of the employed custom QTF and the AmR waist thickness, respectively. The prong spacing of the used custom QTF is ~800 μm and the waist of the AmRs is cut to satisfy the condition: $T < g$. A sharp blade is used to open a pair of slits on each side of the tube waist symmetrically in the middle of the AmR where the acoustic pressure antinode is located. The AmR is assembled at the optimum vertical position h corresponding to a distance of 1.2 mm between the AmR center and the QTF top (12% of the QTF prong length) [16].

The schematic diagram of the experimental setup is depicted in Fig. 2. A 40 mW distributed feedback (DFB) laser (FITEL FRL15DCWD-A82), whose wavelength covers from 1562 nm to 1582 nm, was employed as the excitation light source to generate photoacoustic signals. The wavelength of the laser can be coarsely and finely tuned by scanning its temperature and the current, respectively. The current of the laser was sinusoidally modulated at $f_0/2$, where f_0 was the resonance frequency of the used QTF. The laser beam was collimated to pass through the AmR by a fiber-coupled collimator (OZ optics Ltd. Model LPC-01), which produces a collimated laser beam diameter of ~200 μm with a divergence angle of 9 mrad on the QTF plane. A custom QTF similar to those used in [15,16] was employed to detect the PAS signal. The length, width, and thickness of the used custom QTF prongs were 10 mm,

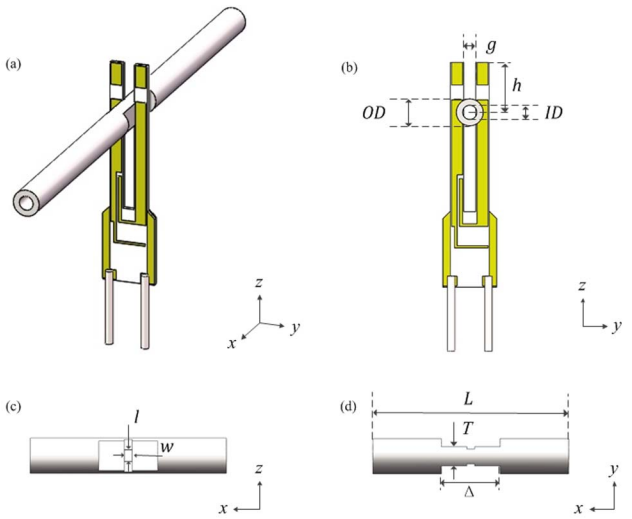

Fig. 1. (a) Schematic of the SO-QEPAS spectrophone; (b), (c), (d) symbols of the geometric parameters of the SO-QEPAS spectrophone, where g is the QTF prong spacing, l is the slit length, w is the slit width, L is the acoustic resonator length, ID is the inner diameter, OD is the outer diameter, T is the waist thickness, and Δ is the waist length.

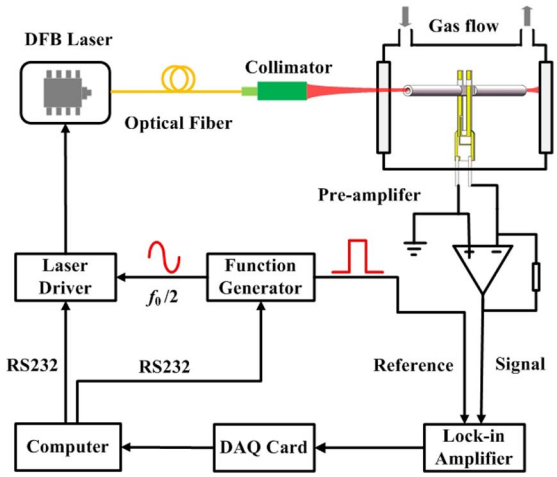

Fig. 2. Schematic diagram of the experimental setup.

0.9 mm, and 0.25 mm, respectively. The resonance frequency, Q factor, and equivalent resistance at atmospheric pressure were 7.207 kHz, 8406, and 299 kΩ, respectively. The custom QTF behaved like a standard QTF transducer in terms of Q factor and resonance frequency [14]. The piezoelectric signal from the QTF was processed by a custom transimpedance amplifier with a 10 MΩ feedback resistance and then applied to a lock-in amplifier (Stanford Research Systems, Model SR830) to demodulate the signal in $2f$ mode, with a time constant of 1 s and a slope filter of 12 dB/octave, corresponding to a detection bandwidth of $\Delta f = 0.25$ Hz.

CO_2 gas was selected as the detection target in a dry standard gas mixture with 5% CO_2 in N_2. The CO_2 absorption line located at 6361.25 cm^{-1} with an intensity of 1.732×10^{-23} $cm \cdot mol^{-1}$ was selected as the target absorption line, using the HITRAN database. The gas flow rate was kept at 200 standard cubic centimeters per minute (sccm). The measurements were carried out at atmospheric pressure and room temperature. Three AmRs with different outer diameters (ODs) and inner diameters (IDs) were chosen to realize the SO-QEPAS spectrophone. The corresponding geometrical parameters of each AmR are listed in Table 1. AmR #1 has a 0.8 mm OD which is equal to the prong spacing (g) of the custom QTF, while AmR #2 and AmR #3 have a larger OD value, but a smaller ID value compared to the prong spacing (g). The waist thicknesses (T) of the AmRs were polished to ~760 μm, as close as possible to the prong spacing (g) of the custom QTF to maximize the acoustic wave coupling efficiency, while the waist length Δ is ~3 mm. The slit width (w) must be smaller than the QTF crystal thickness (250 μm) to ensure that the generated acoustic waves can drive the prongs effectively. The selected slit width (w) was ~90 μm, considering that a larger slit width would disperse the acoustic energy, while a smaller slit size would limit the coupling of the acoustic energy. The optimum slit length (l) for the AmR #1, #2, and #3 were experimentally determined to be 0.24 mm, 0.33 mm, and 0.33 mm, respectively.

It is known that the AmR length has a significant impact on the photoacoustic signals [1,16–19]. Therefore, the lengths of the AmRs were optimized. The AmR lengths were altered from 25 mm (~$\lambda/2$) to 46 mm (~λ), according to the equation $\lambda = v/f$, where λ, v, and f represent the acoustic wavelength,

Table 1. Intercomparison of Three AmRs Used in the SO-QEPAS Spectrophone[a]

		Geometrical Parameters (mm)											
QTF	AmR	OD	ID	L	T	l	Q factor	Signal (μV)	1σ Noise (μV)	SNR	Gain Factor	Power (mW)	NNEA ($cm^{-1} \cdot W/\sqrt{Hz}$)
Custom	AmR #1	0.8	0.55	34	0.76	0.24	7681	232	1.21	191	44	32.2	3.02×10^{-8}
	AmR #2	0.9	0.65	38	0.76	0.33	6682	676	1.22	554	128	37.7	1.21×10^{-8}
	AmR #3	1	0.75	38	0.76	0.33	7528	517	1.34	385	90	38	1.75×10^{-8}
	Bare custom QTF						8406	5	1.16	4.3	1	38	1.59×10^{-6}
	Custom QTF with an optimal traditional on-beam configuration										40 [16]		
Standard	Bare standard QTF						11327	25	1.35	18.5	1	38	3.7×10^{-7}
	Standard QTF with optimal traditional on-beam configuration						5176	605	1.6	378	30 [17]	38	1.8×10^{-8}

[a]The gain factors are calculated as the ratios between the SNRs of the QTF spectrophone and that of a bare QTF, for both custom and standard QTFs.

velocity, and frequency, respectively. Figure 3 depicts the SO-QEPAS signals, obtained by the three different spectrophones listed in Table 1, in logarithmic form as a function of the AmR lengths. The data points were fitted by a Lorentz line shape. The SO-QEPAS spectrophone with AmR #2 demonstrated the strongest signal compared to the other two AmRs, as shown in Fig. 3. The maximum signal amplitudes for the AmR #1, #2, and #3 were obtained at the length of 36 mm, 39 mm, and 38 mm, respectively. These lengths were longer than the half-wavelength of acoustic wave, indicating that the first harmonic acoustic standing waves in the 1D resonator were partially distorted. This is attributed to the two slits present in the resonator, which cause a diverging flow from the AmR. The acoustic pressure distributions in the AmR as a function of the gap of two separated tubes are schematically illustrated in Fig. 4.

The pressure profiles in Fig. 4(a) show that two perfect first longitudinal resonances for two independent half-wavelength solid tubes are generated when the two tubes are well separated. Each tube behaves as an independent half-wavelength resonator. Therefore, there is no acoustic coupling effect between the two tubes. As the two tubes get closer until their gap is approximately equal to the thickness of the QTF prongs, the two resonators become coupled, and, as a result, the two pressure profiles overlap [see Fig. 4(b)]. This case corresponds to the traditional on-beam QEPAS. The optimum full length of the AmR is between $\lambda/2$ and λ, but closer to λ. For example, the acoustic wavelength λ for a custom 7.2 kHz QTF is ~48 mm. The optimum full length of the AmR for the traditional on-beam spectrophone configuration is 46 mm [16]. Note also that the two tubes cannot be located near the QTF; otherwise damping effects start to dominate. When the two tubes are attached together, as shown in Fig. 4(d), the complete system behaves as a single half-wavelength AmR with a full length of $\lambda/2$. For the SO-QEPAS system, two small slits are added on the both sides of the AmR, as shown in Fig. 4(c). Therefore, the resulting acoustic pressure on the QTF is higher with respect to the traditional on-beam spectrophone configuration of Fig. 4(b). Moreover, a shorter AmR than that used in traditional on-beam QEPAS is required.

Figure 5(a) shows the $2f$ signals obtained at atmospheric pressure and room temperature for three SO-QEPAS spectrophones when detecting a dry standard gas mixture with 5% CO_2 in N_2. The three SO-QEPAS spectrophones were constructed with the optimized AmR parameters of ID = 0.55 mm $L = 34$ mm (AmR #1), ID = 0.65 mm $L = 38$ mm (AmR #2), and ID = 0.75 mm $L = 38$ mm (AmR #3), respectively. The obtained Q factors, signal amplitudes, noise (1σ), SNR, and corresponding normalized noise equivalent absorption coefficient (NNEA) are listed in Table 1. The background noise was measured by adjusting the temperature and current of the laser to tune the wavelength far away

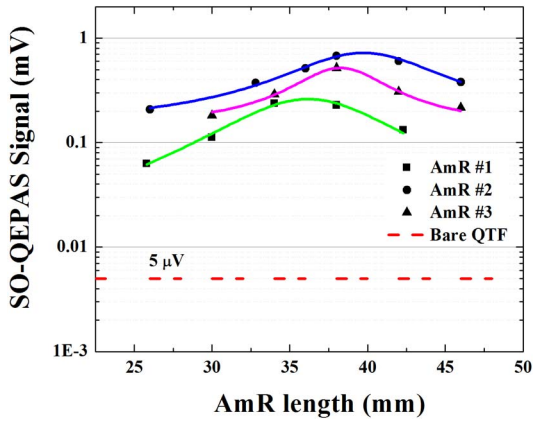

Fig. 3. SO-QEPAS signals obtained by three different spectrophones as a function of AmR lengths.

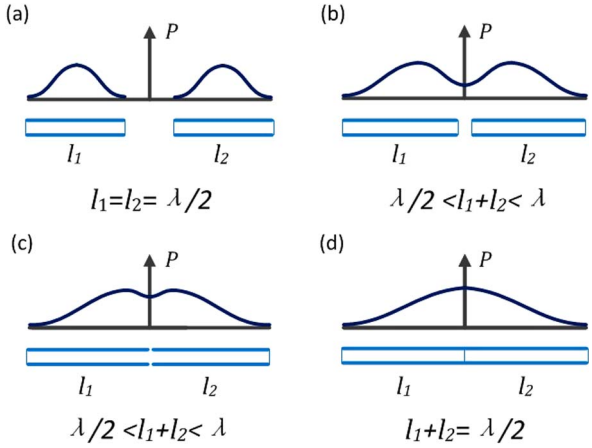

Fig. 4. Schematic of the acoustic pressure distributions in different spectrophone configurations. (a) Two tubes separated by a large gap; (b) traditional on-beam spectrophone configuration; (c) SO-QEPAS spectrophone configuration; (d) traditional acoustic cell.

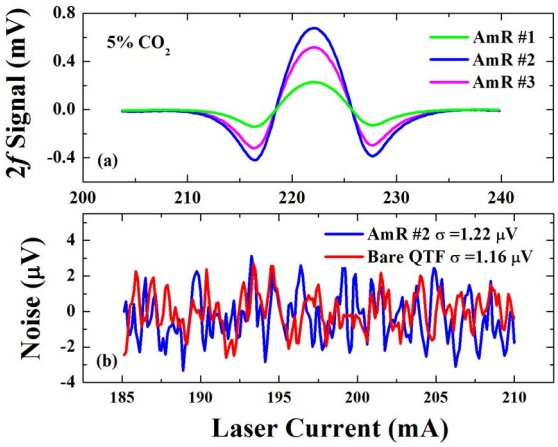

Fig. 5. (a) 5% CO_2 $2f$ signals obtained by three SO-QEPAS spectrophones; (b) noise generated by a SO-QEPAS spectrophone (AmR #2) and a bare custom tuning fork.

from the target CO_2 absorption line. As shown in Table 1, the SO-QEPAS spectrophone with AmR #2 demonstrated the maximum signal amplitude of 676 μV, which is 135 times higher than that of a bare custom QTF. Moreover, the noise level of SO-QEPAS spectrophone with AmR #2, calculated from the standard deviation (1σ), is 1.22 μV, which is comparable to 1.16 μV obtained by the bare custom tuning fork, as shown in Fig. 5(b). A 1σ detection limit of 90 ppm for dry CO_2 detection was obtained by the SO-QEPAS spectrophone with AmR #2 for a 1 s integration time. This detection limit corresponds to a NNEA of 1.21×10^{-8} $cm^{-1} \cdot W/\sqrt{Hz}$.

The optimum signal obtained by the SO-QEPAS spectrophone with AmR #2 shows a SNR gain factor of 128 in comparison with the bare custom QTF, as listed in Table 1. This gain factor was 3 times higher than that obtained by an optimal traditional on-beam QEPAS spectrophone configuration with an identical custom QTF [16]. The large SNR gain factor measured for the SO-QEPAS spectrophone is due to the higher acoustic coupling efficiency between the single-tube AmR and the QTF, making the inner resonant mode more similar to first harmonic acoustic standing waves. Moreover, the SO-QEPAS requires a shorter AmR length, thus facilitating the light alignment and thereby lowering the background noise. The SO-QEPAS with a 26 mm long AmR gives a detection sensitivity comparable to the traditional on-beam QEPAS with a 46 mm long AmR using identical custom QTFs. This means that the spectrophone size can be reduced by 43%, without a decrease of detection sensitivity. This can be crucial in term of background noise reduction when laser beams with poor beam quality or high beam divergence, such as a THz laser beam [14,15] or beams in an intracavity-QEPAS configuration [20], are used in the QEPAS-based sensor systems. The signal amplitude of the bare custom QTF is 5 times less than that of the bare standard QTF due to its large prong spacing and the rapid attenuation of the cylindrically symmetric pressure wave. However, SO-QEPAS has a 4 times higher gain factor and 1.5 higher SNR than the traditional on-beam configuration using a standard QTF, as shown in Table 1.

In conclusion, we have demonstrated a novel QEPAS spectrophone configuration using a single stainless tube and a custom tuning fork, in which the single tube AmR is inserted between the prongs of the QTF to enhance the detection SNR by >100 times in comparison with the bare custom QTF and reaching a sensitivity higher than the traditional on-beam configuration using a standard QTF. Recently, the use of the first overtone mode of custom QTFs, instead of the fundamental mode, results in an enhancement factor of 5 in the detection sensitivity [21]. As the wavelength of the acoustic wave is shorter in the overtone modes, the combination of SO-QEPAS and the overtone resonance modes of custom QTFs is expected to further enhance the detection sensitivity and reduce the QEPAS spectrophone size.

Funding. 973 program (2012CB921603); National Natural Science Foundation of China (NSFC) (61275213, 61475093, 61575113, 61378047); National Science Foundation (NSF) (ERC MIRTHE); Robert Welch Foundation (C-0586); Italian research projects (PON02 00576, PON02 00675, PON03-Sistema).

REFERENCES

1. A. Miklós, P. Hess, and Z. Bozóki, Rev. Sci. Instrum. **72**, 1937 (2001).
2. L. Dong, H. Wu, H. Zheng, Y. Liu, X. Liu, W. Jiang, L. Zhang, W. Ma, W. Ren, W. Yin, S. Jia, and F. K. Tittel, Opt. Lett. **39**, 2479 (2014).
3. A. A. Kosterev, Y. A. Bakhirkin, R. F. Curl, and F. K. Tittel, Opt. Lett. **27**, 1902 (2002).
4. P. Patimisco, G. Scamarcio, F. K. Tittel, and V. Spagnolo, Sensors **14**, 6165 (2014).
5. H. Wu, L. Dong, X. Liu, H. Zheng, X. Yin, W. Ma, L. Zhang, W. Yin, and S. Jia, Sensors **15**, 26743 (2015).
6. H. Wu, L. Dong, H. Zheng, X. Liu, X. Yin, W. Ma, L. Zhang, W. Yin, S. Jia, and F. K. Tittel, Sens. Actuators, B **221**, 666 (2015).
7. H. Zheng, L. Dong, X. Yin, X. Liu, H. Wu, L. Zhang, W. Ma, W. Yin, and S. Jia, Sens. Actuators, B **208**, 173 (2015).
8. Y. Cao, W. Jin, L. H. Ho, and Z. Liu, Opt. Lett. **37**, 214 (2012).
9. M. Köhring, S. Böttger, U. Willer, and W. Schade, Sensors **15**, 12092 (2015).
10. Y. Ma, X. Yu, G. Yu, X. Li, J. Zhang, D. Chen, R. Sun, and F. K. Tittel, Appl. Phys. Lett. **107**, 021106 (2015).
11. H. Yi, R. Maamary, X. Gao, M. W. Sigrist, E. Fertein, and W. Chen, Appl. Phys. Lett. **106**, 101109 (2015).
12. V. Spagnolo, A. A. Kosterev, L. Dong, R. Lewicki, and F. K. Tittel, Appl. Phys. B: Lasers Opt. **100**, 125 (2010).
13. L. Dong, V. Spagnolo, R. Lewicki, and F. K. Tittel, Opt. Express **19**, 24037 (2011).
14. S. Borri, P. Patimisco, A. Sampaolo, H. E. Beere, D. A. Ritchie, M. S. Vitiello, G. Scamarcio, and V. Spagnolo, Appl. Phys. Lett. **103**, 021105 (2013).
15. V. Spagnolo, P. Patimisco, R. Pennetta, A. Sampaolo, G. Scamarcio, M. S. Vitiello, and F. K. Tittel, Opt. Express **23**, 7574 (2015).
16. H. Wu, A. Sampaolo, L. Dong, P. Patimisco, X. Liu, H. Zheng, X. Yin, W. Ma, L. Zhang, W. Yin, V. Spagnolo, S. Jia, and F. K. Tittel, Appl. Phys. Lett. **107**, 111104 (2015).
17. L. Dong, A. A. Kosterev, D. Thomazy, and F. K. Tittel, Appl. Phys. B **100**, 627 (2010).
18. K. Liu, X. Guo, H. Yi, W. Chen, W. Zhang, and X. Gao, Opt. Lett. **34**, 1594 (2009).
19. D. V. Serebryakov, I. V. Morozov, A. A. Kosterev, and V. S. Letokhov, Quantum Electron. **40**, 167 (2010).
20. S. Borri, P. Patimisco, I. Galli, D. Mazzotti, G. Giusfredi, N. Akikusa, M. Yamanishi, G. Scamarcio, P. De Natale, and V. Spagnolo, Appl. Phys. Lett. **104**, 091114 (2014).
21. A. Sampaolo, P. Patimisco, L. Dong, A. Geras, G. Scamarcio, T. Starecki, F. K. Tittel, and V. Spagnolo, Appl. Phys. Lett. **107**, 231102 (2015).